

TEMPERATURE DEPENDENT ELECTRON AND HOLE CAPTURE CROSS SECTIONS OF IRON-CONTAMINATED BORON-DOPED SILICON

B. B. Paudyal¹, K. R. McIntosh¹, D. H. Macdonald²

¹Centre for Sustainable Energy Systems, Australian National University, Canberra, ACT 0200, Australia

²Department of Engineering, Australian National University, Canberra, ACT 0200, Australia

ABSTRACT

Temperature controlled photoconductance is applied to measure the electron and hole capture cross sections of interstitial iron and iron–boron pairs in crystalline silicon. The injection-dependent lifetime was measured before and after light soaking over the range 0–90 °C, and without light soaking over the range 240–320 °C. The data was then analysed to determine the electron and hole capture cross sections of the interstitial iron defect over the range 240–320 °C, and of the iron–boron defect over the range 0–90 °C. The first of these analyses involved a novel approach that independently distinguishes the capture cross sections assuming a known defect density, energy level and thermal velocity, whereas the latter involved the “characteristic cross-over point” method, which compares carrier lifetime before and after the dissociation of iron–boron pairs. This approach independently determines the temperature dependence of the capture cross sections over a wide range of temperature and identifies their capture mechanisms.

INTRODUCTION

Iron (Fe) is one of the most common contaminants in silicon and can occur during crystal growth or wafer processing by either mechanical contact or liquid phase contact with iron-contaminated solutions [1]. Once incorporated into a device, Fe remains in either dissolved or precipitated form. The precipitated Fe in silicon contributes to increased leakage currents and reduced breakdown resistance, which eventually reduces the device performance [1]. Fe dissolved on interstitial lattice sites of silicon is electrically active and affects recombination in silicon and reduces the performance of solar cells. The information on T-dependent carrier capture cross sections of dissolved Fe in silicon helps to identify the capture mechanisms and find possible ways to minimize its effect on recombination in silicon. Furthermore the T-dependence of the capture cross section ratio (σ_n / σ_p) also helps to resolve the ambiguity in previous results obtained by temperature-dependent lifetime spectroscopy (TDLS) analyses that assumed σ_n / σ_p to be temperature independent.

Dissolved Fe in silicon exhibits a donor level Fe_i^{+0} in the lower half of the band gap ($E_v + 0.39$ eV), as detected by deep level transient spectroscopy (DLTS) by various researchers and summarized by Graff [1] and Istratov *et al.* [2]. The energy level of Fe_i^{+0} is below the valence band and has no direct effect on carrier recombination. In boron-doped silicon, positively charged Fe_i atoms form pairs with

negatively charged substitutional boron (B^-) by coulombic attraction. This state gives rise to a donor level FeB^{+0} in the lower band half ($E_v + 0.1$ eV), and an acceptor level FeB^{0-} in the upper band half ($E_c - 0.27$ eV) of silicon [1-3]. These three defect energy levels within the band gap of Fe-contaminated, boron-doped silicon act as recombination centres [2]. Figure 1 depicts the energy level of Fe_i^{+0} , FeB^{+0} and FeB^{0-} in the band gap of silicon.

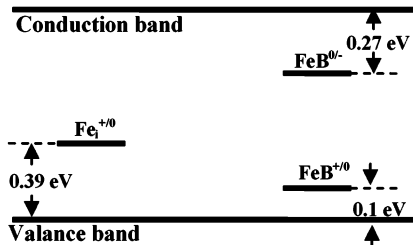


Fig. 1. Energy levels in silicon depicting $E_t(Fe_i^{+0})$, $E_t(FeB^{+0})$ and $E_t(FeB^{0-})$.

The defect energy E_t of the above mentioned defects has been measured and reported by various researchers using different techniques and found to be quite consistent. However, the reported values for their capture cross sections (σ_n and σ_p) and the dependence of σ_n and σ_p on temperature are inconsistent, as summarised by Table 1.

The T dependence of $\sigma_p(Fe)$ was first determined by Induskar *et al.* [4] in 1966 using DLTS followed by Wunstel *et al.* [5] in 1982 and Brotherton *et al.* [6] in 1984. Their results conclude the multi-phonon emission (MPE) capture [7] to be the effective mechanism for hole capture, but there is some disagreement in their values for the activation energy E_a (varies from 0.040 to 0.048 eV) and the T-independent pre-factor σ_∞ (varies from 1.6×10^{-16} to 6.8×10^{-16}). On the other hand $\sigma_n(Fe_i)$ has not been studied by as many researchers as $\sigma_p(Fe_i)$. The first result on $\sigma_n(Fe_i)$ at room temperature was published by Collins *et al.* [8] in 1957 followed by Zoth *et al.* [9] in 1990 and Lagowski *et al.* [10] in 1993. Their experiments were based upon surface photo-voltage (SPV) with the photo-dissociation technique and reported different values for $\sigma_n(Fe_i)$ at room temperature. Later in 1999, Graff [1] presented a T-dependent expression for $\sigma_n(Fe_i)$ in his text by taking the average of reported results from different researchers. However this T-dependent expression presented by Graff [1] does not lead to the same $\sigma_n(Fe_i)$ at room temperature published by Zoth *et al.* [9].

Table 1. Summary of results

$\sigma_p(Fei)$	$\sigma_n(Fei)$	$\sigma_p(FeB)$	$\sigma_n(FeB)$	Ref and Technique
$4.54 \times 10^{-16} \exp(-0.05/k_B T)$	$3.47 \times 10^{-11} \times T^{-1.48}$	$3.32 \times 10^{-11} \exp(-0.262/k_B T)$	$5.1 \times 10^{-9} \times T^{-2.5}$	This work, TIDLS
$6.8 \times 10^{-16} \exp(-0.04/k_B T)$	-----	-----	-----	[4], TSCAP & DLTS
$5.6 \times 10^{-16} \exp(-0.048/k_B T)$	-----	-----	-----	[6], DLTS
$1.6 \times 10^{-16} \exp(-0.043/k_B T)$	-----	-----	-----	[5], DLTS & Hall
$2.8 \times 10^{-16} \exp(-0.043/k_B T)$	$10^{-10} \times T^{-1.5}$	2.0×10^{-15} at 400 K	1.6×10^{-15}	[1], Average of [6, 9, 11]
$3.9 \times 10^{-16} \exp(-0.045/k_B T)$	4×10^{-14}	3×10^{-14}	2.5×10^{-14}	[2], Average of [4-6]
-----	-----	5.4×10^{-15} at 90K	1.8×10^{-15} at 90K	[11], DLTS
-----	-----	3×10^{-14}	2.5×10^{-15}	[12] SPV & ELYMAT
-----	-----	1.1×10^{-15}	1.4×10^{-14}	[13], CoP & TIDLS
-----	3.6×10^{-15}	5.5×10^{-15}	2.5×10^{-15}	[14], TIDLS
-----	-----	3×10^{-15}	5×10^{-14}	[15], CoP & IDLS
-----	$\geq 1.5 \times 10^{-15}$	-----	-----	[8], Hall and Lifetime
-----	2.6×10^{-14}	-----	4×10^{-13}	[9, 10], SPV

*Reported values are for room temperature (300 K) unless otherwise specified

Wunstel *et al.* [5] applied DLTS for the temperatures between 50 K and 65 K followed by Gao *et al.* [16] at the temperature 55 K to measure $\sigma_p(FeB)$ and published the result in 1982 and 1991, respectively; neither investigated the thermal activation. Lemke *et al.* [11] reported the value of $\sigma_p(FeB)$ and $\sigma_n(FeB)$ at 90 K applying DLTS. Later Zoth *et al.* [9] reported $\sigma_n(FeB)$ at room temperature using DLTS with SPV techniques. Walz *et al.* [12, 17] reported $\sigma_n(FeB)$ and $\sigma_p(FeB)$ at room temperature using SPV and the ELYMAT technique. Birkholz *et al.* [13] applied the crossover point (CoP) technique with photoconductance measurements and devices, reporting $\sigma_n(FeB)$ and $\sigma_p(FeB)$ for FeB. Later Paudyal *et al.* [18] applied a similar technique to determine the T-dependent expression and the effective capture mechanism of $\sigma_n(FeB)$ and $\sigma_p(FeB)$ for FeB. These reported results are mostly based upon relatively complex techniques and only gives the value at room temperature. Furthermore the T-dependent expressions reported by Paudyal *et al.* [18] for $\sigma_n(FeB)$ was based upon the T-dependent models for the averaged $\sigma_n(Fei)$ and $\sigma_p(FeB)$ suggested by Graff [1].

Hence, accurate and self-consistent T-dependent expressions for $\sigma_n(Fei)$, $\sigma_p(Fei)$, $\sigma_n(FeB)$ and $\sigma_p(FeB)$ have not yet been agreed upon. This paper presents a novel and relatively simple technique for the determination of T-dependent expressions for these parameters using temperature and injection-dependent lifetime spectroscopy (TIDLS) analysis with a temperature-controlled photoconductance (PC) measurement instrument. We first explain the carrier lifetime theory and its simplification in order to determine the temperature-dependent expression for σ_n and σ_p for Fei and FeB. This is followed by an experimental section that presents the details of the samples used in this work, the temperature-controlled PC measurement procedure, and the results obtained by the implementation of TIDLS analysis and their comparison to the previously reported values and

expressions. Finally, we discuss the effective capture mechanism for all four carrier capture processes.

THEORY AND BACKGROUND

FeB pairs form in boron-doped silicon due to coulombic attraction between a positively charged interstitial Fe (Fe_i^+) and a negatively charged boron atom (B^-). Such a coulombic bond can be broken by the external supply of optical, thermal or electrical energy which dissociates the FeB pairs back to isolated Fe_i^+ and B^- atoms. The temperature at which a complete thermal dissociation (T_{CTD}) of FeB pairs occurs is dependent upon the concentration of boron (N_A) and Fe in silicon. Figure 2 depicts the Arrhenius plot of a boron-doped Fe-contaminated $1.0 \Omega cm$ wafer at $\Delta n = 5 \times 10^{13} cm^{-3}$, which illustrates the T_{CTD} at $235^\circ C$ and the effect of Fei and FeB on the carrier lifetime. Hence the analysis of effective lifetime measurements at temperatures higher than T_{CTD} gives parameters for Fei defects only.

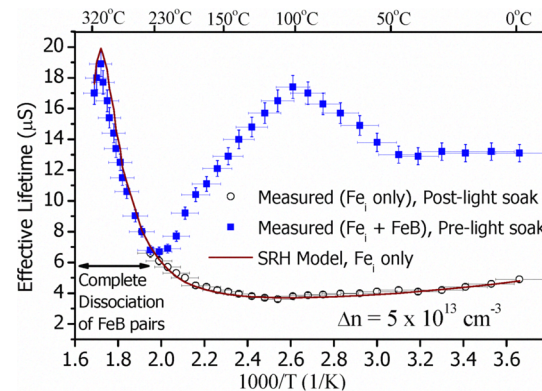


Fig. 2. Arrhenius plot of $1.0 \Omega cm$ depicting the complete thermal dissociation temperature (T_{CTD}) for FeB pairs and the effect of Fei and FeB in Silicon.

The simplified version of Shockley Read Hall (SRH) lifetime [19, 20] for a single defect without any traps (i.e. $\Delta n = \Delta p$) can be written as [21],

$$\tau_{SRH} = \frac{\tau_{n_0}(p_1 + p_0 + \Delta n) + \tau_{p_0}(n_1 + n_0 + \Delta n)}{(n_0 + p_0 + \Delta n)}, \quad (1)$$

where τ_{n_0} and τ_{p_0} are the fundamental capture time constants for electrons and holes, $n_1 = N_C \exp[(E_c - E_i)/k_B T]$ and $p_1 = N_V \exp[(E_i - E_v)/k_B T]$, N_C and N_V are the effective densities of states at the conduction and valance band edge, k_B is Boltzmann's constant, n_0 and p_0 are the electron and hole densities at thermal equilibrium, and Δn is the excess carrier density.

T-dependent values of $\sigma_n(Fe_i)$ and $\sigma_p(Fe_i)$

For a *p*-type wafer n_0 can be neglected in comparison to p_0 and when Δn is sufficiently less than p_0 , the SRH equation can be simplified to

$$\tau_{SRH} = \frac{\tau_{n_0}(p_1 + p_0) + \tau_{p_0}(n_1 + n_0)}{p_0} + \frac{\tau_{p_0}}{p_0} \Delta n. \quad (2)$$

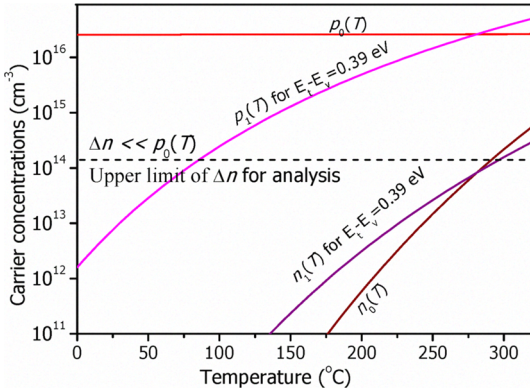


Fig. 3. Carrier densities $p_0(T)$, $p_1(T)$, $n_0(T)$ and $n_1(T)$ for the temperature range 270 to 600 K for $\Delta E_t = 0.391$ eV and $N_A = 2.6 \times 10^{16} \text{ cm}^{-3}$. Depicts the upper limit of $\Delta n \ll p_0(T)$ for TIDLS analysis.

The slope of a linear plot of τ_{eff} against Δn therefore gives τ_{p_0}/p_0 and the intercept gives $[\tau_{n_0} \times (p_1 + p_0) + \tau_{p_0} \times (n_1 + n_0)]/p_0$. Under conditions when the Fe_i defect dominates over all other recombination process i.e. above T_{CTD} temperature, p_1 and n_1 can be calculated for any temperature using $E_{t(Fe_i)}$. The corresponding p_0 and n_0 can be calculated using doping density N_A and intrinsic carrier concentration (n_i). Hence τ_{n_0} and τ_{p_0} can be calculated using the measured slope of the linear plot and corresponding values of p_1 , n_1 , p_0 and n_0 at different temperatures. The $\sigma_n(Fe_i)$ and $\sigma_p(Fe_i)$ can then be determined by using equation (3) and (4) using known values of the slope and intercept, the T-dependent value of the thermal velocity, and the Fe_i concentration (N_i).

$$\sigma_p = \frac{1}{\tau_{p_0} v_{th} N_T} = \frac{1}{slope \times p_0 v_{th} N_T} \quad (3)$$

$$\sigma_n = \frac{1}{\tau_{p_0} v_{th} N_T} = \frac{p_1 + p_0}{[Intercept - slope \times (n_1 + n_0)] \times p_0 v_{th} N_T} \quad (4)$$

T-dependent values of $\sigma_n(FeB)$ and $\sigma_p(FeB)$

The density of Fe_i and FeB below T_{CTD} can be altered in boron-doped silicon by dissociating FeB pairs. Despite variations in the population of Fe_i and FeB , the effective lifetime remains unchanged at a particular excess carrier density known as the characteristic crossover point (CoP) [3, 13]. CoP is depicted in Figure 3 for $0.6 \Omega \text{ cm}$ at 50°C . The CoP carrier density (Δn_{CoP}) is independent with degree of dissociation of FeB pairs and only depends upon the temperature and N_A . Hence at CoP, if we consider solely Shockley-Read-Hall recombination [19, 20], the lifetime (τ_{CoP}) at Δn_{CoP} can be simplified as,

$$\begin{aligned} \frac{1}{\tau_{CoP}} &= \frac{1}{\tau_{associated}} = \frac{1}{\tau_{dissociated}} = \frac{1}{\tau_{SRH,as(FeB)}} + \frac{1}{\tau_{SRH,as(Fei)}} \\ &= \frac{1}{\tau_{SRH,dis(FeB)}} + \frac{1}{\tau_{SRH,dis(Fei)}} \end{aligned} \quad (5)$$

where, τ_{as} denotes the associated and τ_{dis} denotes the dissociated lifetime at the crossover point. Birkholz *et al* [13] solved equation (5) for Δn_{CoP} for *p*-type boron-doped silicon when $n_1(Fe_i)$, $p_1(Fe_i)$, $p_1(FeB)$ and n_0 can be neglected in comparison to p_0 , giving,

$$\begin{aligned} \Delta n_{CoP} &= \frac{\sigma_n^{-1}(FeB) - \sigma_n^{-1}(Fe_i)}{\sigma_p^{-1}(Fe_i)} p_0 \\ &+ \frac{\sigma_p(Fe_i)}{\sigma_p(FeB)} N_C \exp\left(-\frac{E_c - E(FeB)}{kT}\right) \end{aligned} \quad (6)$$

Therefore, from the slope and intercepts of the linear plot of Δn_{CoP} versus p_0 at different temperatures, and with the values of $\sigma_n(Fe_i)$, $\sigma_p(Fe_i)$, N_C , and $E(FeB)$, T-dependent values for $\sigma_n(FeB)$ and $\sigma_p(FeB)$ can be determined.

EXPERIMENTS

The experiment was performed on four boron-doped silicon samples with resistivities 0.6, 1, 5.5 and $13 \Omega \text{ cm}$. The average widths of the samples were 250, 490, 199 and 445 microns respectively. Those samples had been intentionally contaminated with Fe by ion implantation with an implant dose of $1 \times 10^{11} \text{ cm}^{-2}$. After implantation the samples were annealed at 900°C for one hour in order to obtain a uniform distribution of Fe throughout the bulk. The dose is then divided by the width of the wafer to calculate the Fe concentration within the bulk. In all cases the Fe concentration is below the solubility limit of Fe at 900°C so that there should be very few Fe atoms in precipitate form. Furthermore each sample was coated with plasma enhanced chemical vapour deposition PECVD silicon nitride in order to ensure that the surface recombination was negligible relative to the bulk recombination [21]. Lifetime measurements were performed on a temperature

controlled inductive coil PC based device, described in detail elsewhere [22].

The lifetime measurement technique itself is the well established quasi-steady-state photoconductance technique [23]. The subsequent analysis employed the carrier mobility model developed by Reggiani *et al.* [24], which states how the mobility in equilibrium depends on temperature and dopant concentration. It was modified to account for the injection of Δn by replacing the donor N_D and acceptor N_A concentrations with $N_D + \Delta n$ and $N_A + \Delta n$. When $\Delta n \leq N_A$ (or N_D), this approximation was found to give good agreement with Klaassen's mobility model [25, 26] which does account for Δn . Reggiani's model was preferred to Klaassen's in this case because of its larger temperature range. The temperature across the wafer was found to vary by 2% during measurement, and the uncertainty in lifetime was $\pm 6\%$ [22], which mostly depends on the calibration of the illumination intensity and inductive coil. The effective lifetime T_{eff} was measured as a function of the excess carrier density Δn for each wafer over the temperature range 0–90 °C and 230–320 °C. The equilibrium concentration for electrons n_0 was calculated using N_A and T-dependent model of intrinsic carrier concentration $n_0(T)$ suggested by Green *et al.* [27].

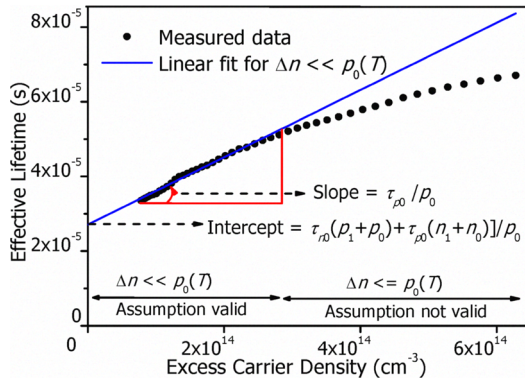


Fig. 4. Measured lifetime data depicting linearity with the fitted model for $\Delta n \ll p_0$ according to Equation 2.

T_{CTD} on 1.0 Ω cm was achieved by heating the sample above 240 °C, which ensures the complete domination of the Fe_i defect on overall recombination process as illustrated in Figure 2. Figure 4 depicts the linearity with the fitted model according to Equation (2) with the measured data for $\Delta n \ll p_0$. Hence the injection-dependent lifetime time measurement for the temperature range 240 to 320 °C were taken and analysed for the determination of $\sigma_p(Fe_i)$ and $\sigma_p(Fe_i)$. Measured lifetime become inconsistent above 320 °C as the intrinsic conduction begins in the sample.

Light soaking technique was applied for a partial dissociation of FeB pairs in all four samples in order to determine Δn_{CoP} for different temperatures. Lifetime measurements were taken before (τ_{as}) and after (τ_{dis}) the light soaking for each temperature. Samples were illuminated by a 25 W halogen lamp for two minutes in a temperature controlled stage of the PC measurement device for light soaking. All samples were kept in dark for two hours before taking the next

measurement in order to repair a significant fraction of broken FeB pairs by the light soaking. The experiment was repeated from 0 to 90 °C at 10 °C steps for all samples. 90 °C is selected as the upper limit for CoP analysis in order to satisfy the condition $n_1(Fe_i)$, $p_1(Fe_i)$, $p_1(FeB)$ and $n_0 \ll p_0$ for all samples under test. Injection-dependent lifetime curve and CoP at 50 °C 1 Ω cm sample and the control sample (1 Ω cm sample without Fe contamination) is depicted in Figure 5.

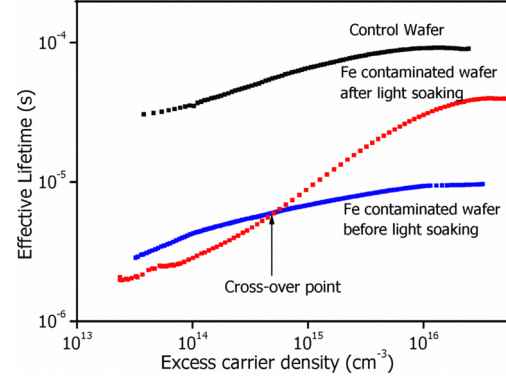


Fig. 5. Effective lifetime measured for 1.0 Ω cm sample at 50 °C, depicts the difference in recombination lifetime of Fe-contaminated wafer with the control wafer and the cross-over point.

RESULT AND DISCUSSIONS

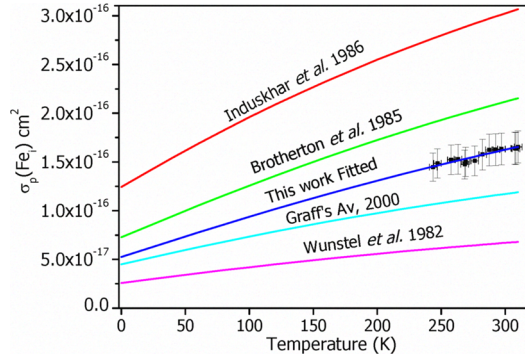


Fig. 6. T-dependent relation for $\sigma_p(Fe_i)$ with reported model.

The measured $\sigma_p(Fe_i)$ for the temperature range 240–320 °C shows an increase with temperature which suggests that MPE is the only effective capture mechanism, consistent with previously reported capture mechanism [1, 2, 4–6]. However, we find different values for the activation energy (E_a) of 0.05 ± 0.006 eV and temperature independent pre-factor (σ_∞) equals to $4.54 \pm 0.5 \times 10^{-16}$ cm². The errors for the results in this work are estimated from the best-fit of the measured data to the equation of the reported capture mechanisms [7, 28, 29]. The MPE capture expression obtained in this work is extended to 0 °C and depicted in Figure 6 along with the expressions reported by others.

$$\sigma_{p(Fe_i)} = 4.54 \times 10^{-16} \exp\left(-\frac{0.05}{k_B T}\right) \quad (7)$$

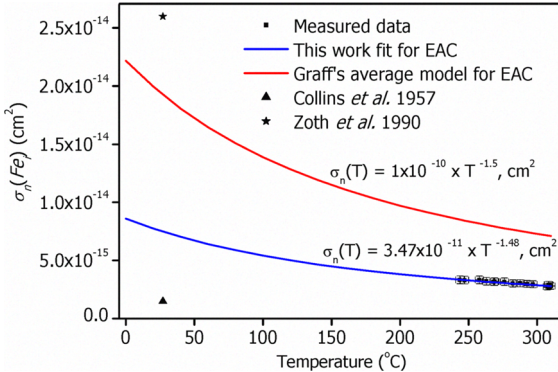


Fig. 7. T-dependent relation for $\sigma_n(Fe_i)$ with other reported model and values at room temperature.

The measured T-dependent data for $\sigma_n(Fe_i)$ over the temperature range 240 – 320 °C decreased with temperature. Hence MPE capture mechanism can be ruled out. Instead, the data shows a better fit to the negative power relation to temperature, consistent with the capture mechanism being either cascade capture [28] or excitonic Auger (EA) capture [29]. As the defect level of Fe_i is treated as deep, the cascade capture is unlikely in this case. Hence we fitted the measured data for $\sigma_n(Fe_i)$ for EA capture mechanism give the T-independent pre-factor, $\sigma_0 = 3.47 \pm 0.5 \times 10^{-11}$ and the correlation exponent, $\alpha = 1.48 \pm 0.02$. T-dependent expression for $\sigma_n(Fe_i)$ has rarely been reported compared to $\sigma_p(Fe_i)$. Graff [1] reported T-dependent expression for $\sigma_n(Fe_i)$ by taking average value from various works [6, 9, 11]. Figure 7 depicts the expression for $\sigma_n(Fe_i)$ obtained by this work is extended to 0–320 °C along with the other previously reported values of $\sigma_n(Fe_i)$ at room temperature.

$$\sigma_{n(Fe_i)} = 3.47 \times 10^{-11} \times T^{-1.48} \quad (8)$$

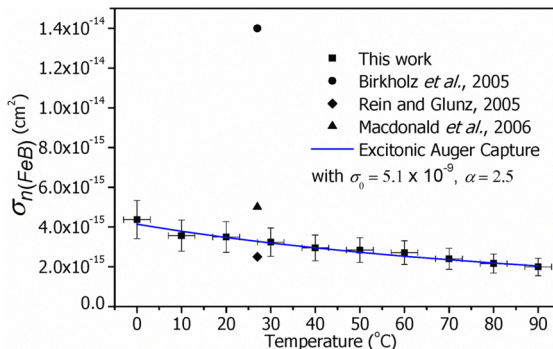


Fig. 8. Electron capture cross-section of FeB pairs for 0 – 90 °C, measured data and Excitonic Auger capture model fit.

$\sigma_n(FeB)$ and $\sigma_p(FeB)$ calculated on the basis of T-dependent expressions determined earlier for $\sigma_n(Fe_i)$ and $\sigma_p(Fe_i)$ and using the measured slope and intercepts of the linear plot of Δn_{CoP} versus doping density (p_0) for the temperature range 0 – 90 °C. $\sigma_n(FeB)$ was found to decrease with the increase in

temperature and comparable with the values reported by Macdonald et al. [15] and Rein et al. [14] at room temperature. The T-dependent trend of $\sigma_n(FeB)$ resembles the T-dependent trend of $\sigma_n(Fe_i)$ and shows a better fit to the excitonic Auger capture mechanism due to deep centres [29]. Figure 8 depicts the plot of excitonic Auger capture with the T-independent pre-factor, $\sigma_0 = 5.1 \pm 1.3 \times 10^{-9}$ and the correlation exponent, $\alpha = 2.5 \pm 0.05$ as per expression (9),

$$\sigma_{n(FeB)} = 5.1 \times 10^{-9} T^{-2.5} \quad (9)$$

Similarly, $\sigma_p(FeB)$ was found to increase with temperature over the temperature range 0 – 90 °C and the measured data is comparable with reported data by Birkholz et al. [13] however less than the values reported by Macdonald et al. [15] and Rein et al. [14] at room temperature as depicted in Figure 9. The T-dependent trend of $\sigma_p(FeB)$ is increasing with temperature. Hence the only possible capture mechanism is MPE capture as depicted in expression (10) with $E_a = 0.262 \pm 0.012$ eV and $\sigma_0 = 3.32 \pm 1.22 \times 10^{-11}$ cm². Table 1 shows the reported values and expressions for $\sigma_p(Fe_i)$, $\sigma_n(Fe_i)$, $\sigma_p(FeB)$ and $\sigma_n(FeB)$.

$$\sigma_{p(FeB)} = 3.32 \times 10^{-10} \exp\left(-\frac{0.262}{k_B T}\right) \quad (10)$$

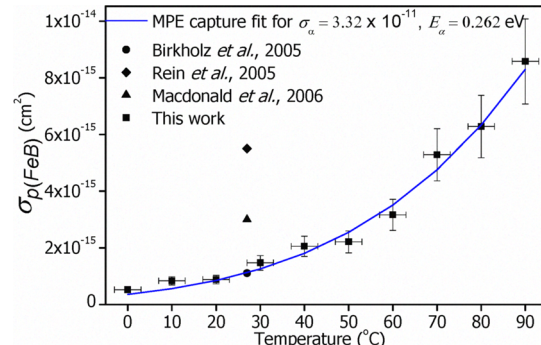


Fig. 9. Hole capture cross-section of FeB pairs for 0 – 90 °C, measured data and Multi-phonon emission capture model fit.

CONCLUSION

T-dependent expressions for the electron and hole capture cross sections of Fe_i and FeB pairs in crystalline silicon has been measured using temperature and injection control lifetime spectroscopy. The most likely capture mechanisms were discussed. The approach for determination of $\sigma_n(Fe_i)$ and $\sigma_p(Fe_i)$ is an alternative to DLTS measurement. Furthermore, it allows measuring the capture cross section regardless of the position of E_t in the band gap of the silicon. The measured data are comparable with some previously reported values, however the measured data are based upon the T-dependent model for n_i , v_{thn} and v_{thp} , so the inaccuracy in these employed T-dependent models have direct effect on the measured results. A better accuracy and confidence could be achieved by measuring different samples prepared in different

batches and doping densities and a comprehensive error analysis in curve fitting.

ACKNOWLEDGEMENT

This work was funded by an Australian Research Council Linkage Grant between the Australian National University, SierraTherm Production Furnaces, and SunPower Corporation. D. M. is supported by an Australian Research Council fellowship.

REFERENCES

- [1] K. Graff, *Metal Impurities in Silicon-Device Fabrication*, Second ed. vol. 24. Berlin: Springer, 1999.
- [2] A. A. Istratov, H. Hieslmair, and E. R. Weber, "Iron and its complexes in silicon," *Appl Phys A: Mat. Sci & Pro*, vol. 69, pp. 13-44, 1999.
- [3] S. Rein, *Lifetime Spectroscopy - A Method of Defect Characterization in Silicon for Photovoltaic Applications* vol. 85. Berlin: Springer, 2005.
- [4] H. Indusekhar and V. Kumar, "Properties of iron related quenched-in levels in p-silicon," *Phys. status solidi (a)*, vol. 95, pp. 269 - 278, 1986.
- [5] K. Wunstel and P. Wagner, "Interstitial Iron and Iron-Acceptor Pairs in Silicon," *Appl. Phys. A*; vol. 27, p. 207, 1982.
- [6] S. D. Brotherton, P. Bradley, and A. Gill, "Iron and the iron-boron complex in silicon," *JAP*, vol. 57, pp. 1941-1943, 1985.
- [7] C. H. Henry and D. V. Lang, "Nonradiative capture and recombination by multiphonon emission in GaAs and GaP," *Phy. Rev. B*, vol. 15, p. 989, 1977.
- [8] C. B. Collins and R. O. Carlson, "Properties of Silicon Doped with Iron or Copper," *Phy. Rev.*, vol. 108, p. 1409, 1957.
- [9] G. Zoth and W. Bergholz, "A fast, preparation-free method to detect iron in silicon," *JAP*, vol. 67, pp. 6764-6771, 1990.
- [10] J. Lagowski, P. Edelman, A. M. Kontkiewicz, O. Milic, W. Henley, M. Dexter, L. Jastrzebski, and A. M. Hoff, "Iron detection in the part per quadrillion range in silicon using surface photovoltage and photodissociation of iron-boron pairs," *Appl. Phys. Lett.*, vol. 63, pp. 3043-3045, 1993.
- [11] H. Lemke, "Dotierungseigenschaften von Eisen in Silizium," *Phys. status solidi (a)*, vol. 64, pp. 215-224, 1981.
- [12] D. Walz, J. P. Joly, and G. Kamarinos, "On the recombination behaviour of iron in moderately boron-doped p-type silicon," *Appl. Phys. A*; vol. 62, pp. 345-353, 1996.
- [13] J. E. Birkholz, K. Bothe, D. Macdonald, and J. Schmidt, "Electronic properties of iron-boron pairs in crystalline silicon by temperature- and injection-level-dependent lifetime measurements," *JAP*, vol. 97, 2005.
- [14] S. Rein and S. W. Glunz, "Electronic properties of interstitial iron and iron-boron pairs determined by means of advanced lifetime spectroscopy," *JAP*, vol. 98, p. 113711, 2005.
- [15] D. Macdonald, T. Roth, P. N. K. Deenapanray, T. Trupke, and R. A. Bardos,
- [16] "Doping dependence of the carrier lifetime crossover point upon dissociation of iron-boron pairs in crystalline silicon," *Appl. Phys. Lett.*, vol. 89, p. 142107, 2006.
- [17] X. Gao, H. Mollenkopf, and S. Yee, "Annealing and profile of interstitial iron in boron-doped silicon," *Appl. Phys. Lett.*, vol. 59, pp. 2133-2135, 1991.
- [18] D. Walz, G. L. Carval, J. P. Joly, and G. Kamarinos, "An in-depth analysis of the ELYMAT technique for characterizing metallic micro contamination in silicon: experimental validation for iron contamination in p-type silicon," *Semicon. Sci. Tech.*, vol. 10, p. 1022, 1995.
- [19] B. B. Paudyal, K. R. McIntosh, and D. H. Macdonald, "Electron capture cross section of iron-boron pairs in crystalline silicon over the temperature range 0 – 100 °C," in *23rd EU PV SEC, 1-5 September 2008*, Valencia, Spain, 2008, p. 1481.
- [20] W. Shockley and W. T. Read, "Statistics of the Recombinations of Holes and Electrons," *Phys. Rev.*, vol. 87, p. 835, 1952.
- [21] R. N. Hall, "Electron-Hole Recombination in Germanium," *Phy. Rev.*, vol. 87, p. 387, 1952.
- [22] A. G. Aberle, *Crystalline Silicon Solar Cells: Advanced Surface Passivation and Analysis*: Centre for PV Engineering, University of NSW, Sydney NSW 2052, Australia, 1999.
- [23] B. B. Paudyal, K. R. McIntosh, D. H. Macdonald, B. S. Richards, and R. A. Sinton, "The implementation of temperature control to an inductive-coil photoconductance instrument for the range of 0-230°C," *Prog. in PV: Res. and Appl.*, vol. 16, pp. 609-613, 2008.
- [24] R. A. Sinton, A. Cuevas, and M. Stuckings, "Quasi-steady-state photoconductance, a new method for solar cell material and device characterization," in *PV Specialists Conference, 1996., Conference Record of the Twenty Fifth IEEE*, 1996, pp. 457-460.
- [25] S. Reggiani, M. Valdinoci, L. Colalongo, M. Rudan, G. Baccarani, A. D. Stricker, F. Illien, N. Felber, W. Fichtner, and L. Zullino, "Electron and hole mobility in silicon at large operating temperatures. I. Bulk mobility," *Elect. Dev., IEEE Tr. on Elec. Dev.*, vol. 49, pp. 490-499, 2002.
- [26] D. B. M. Klaassen, "A unified mobility model for device simulation-I, Model equations and concentration dependence," *Solid-State Electronics*, vol. 35, pp. 953-959, 1992.
- [27] D. B. M. Klaassen, "A unified mobility model for device simulation-II, Temperature dependence of carrier mobility and lifetime," *Solid State Electron*, vol. 35, pp. 961-967, 1992.
- [28] M. A. Green, "Intrinsic concentration, effective densities of states, and effective mass in silicon," *JAP*, vol. 67, pp. 2944-2954, 1990.
- [29] M. Lax, "Cascade Capture of Electrons in Solids," *Phys. Rev.*, vol. 119, p. 1502, 1960.
- [30] A. Hangleiter, "Nonradiative recombination via deep impurity levels in silicon: Experiment," *Phy. Rev. B*, vol. 35, p. 9149, 1987.